doi:10.1093/brain/awx144 BRAIN 2017: 140; 2193–2209 | 2193

BRAIN
A JOURNAL OF NEUROLOGY

Modelling *APOE* ε3/4 allele-associated sporadic Alzheimer's disease in an induced neuron

Hongwon Kim,[1] Junsang Yoo,[1] Jaein Shin,[1] Yujung Chang,[1] Junghyun Jung,[2] Dong-Gyu Jo,[3] Janghwan Kim,[4,5] Wonhee Jang,[2] Christopher J. Lengner,[6] Byung-Soo Kim[7] and Jongpil Kim[1]

The recent generation of induced neurons by direct lineage conversion holds promise for *in vitro* modelling of sporadic Alzheimer's disease. Here, we report the generation of induced neuron-based model of sporadic Alzheimer's disease in mice and humans, and used this system to explore the pathogenic mechanisms resulting from the sporadic Alzheimer's disease risk factor apolipoprotein E (*APOE*) ε3/4 allele. We show that mouse and human induced neurons overexpressing mutant amyloid precursor protein in the background of *APOE* ε3/4 allele exhibit altered amyloid precursor protein (APP) processing, abnormally increased production of amyloid-β_{42} and hyperphosphorylation of tau. Importantly, we demonstrate that *APOE* ε3/4 patient induced neuron culture models can faithfully recapitulate molecular signatures seen in *APOE* ε3/4-associated sporadic Alzheimer's disease patients. Moreover, analysis of the gene network derived from *APOE* ε3/4 patient induced neurons reveals a strong interaction between *APOE* ε3/4 and another Alzheimer's disease risk factor, desmoglein 2 (*DSG2*). Knockdown of *DSG2* in *APOE* ε3/4 induced neurons effectively rescued defective APP processing, demonstrating the functional importance of this interaction. These data provide a direct connection between *APOE* ε3/4 and another Alzheimer's disease susceptibility gene and demonstrate in proof of principle the utility of induced neuron-based modelling of Alzheimer's disease for therapeutic discovery.

1 Laboratory of Stem Cells and Cell reprogramming, Department of Biomedical Engineering (BK21 plus team), Dongguk University, Seoul, 100-715, Republic of Korea
2 Department of Life Science, Dongguk University, Seoul 100-715, Republic of Korea
3 School of Pharmacy, Sungkyunkwan University, Suwon 440-746, Republic of Korea
4 Stem Cell Research Center, Korea Research Institute of Bioscience and Biotechnology (KRIBBB), Daejeon 305-806, Republic of Korea
5 Department of Functional Genomics, KRIBB School of Bioscience, Korea University of Science and Technology (UST), Daejeon, Republic of Korea
6 Department of Biomedical Sciences, School of Veterinary Medicine and Institute for Regenerative Medicine, University of Pennsylvania, Philadelphia, Pennsylvania 19104, USA
7 School of Chemical and Biological Engineering, Seoul National University, Seoul 151-744, Republic of Korea

Correspondence to: Jongpil Kim, PhD
Associate Professor
Department of Biomedical Engineering
Dongguk University, Seoul, Korea
E-mail: jpkim153@dongguk.edu

Keywords: Alzheimer's disease; amyloid-β; neuroprotection; APP; APOE

Received January 4, 2017. Revised April 7, 2017. Accepted May 7, 2017. Advance Access publication July 3, 2017

Introduction

Alzheimer's disease is the most common neurodegenerative disorder, characterized by cognitive decline with the loss of memory (Selkoe, 2002; Vetrivel *et al.*, 2008). The major pathological features of Alzheimer's disease include the accumulation of amyloid aggregates and hyperphosphorylation of tau protein (Selkoe, 2005). Known mutations causing Alzheimer's disease act either by increasing the steady-state level of amyloid-β, altering the amyloid-$\beta_{42/40}$ ratio or altering the amyloidogenic potential of amyloid-β, which eventually leads to disease pathogenesis (Citron *et al.*, 1998). Particularly, mutations in the amyloid precursor protein (*APP*), presenilin 1 (*PSEN1*) and presenilin 2 (*PSEN2*) genes cause an amino acid substitution in the sites at which the APP is cleaved, leading to accumulation of mainly amyloid-β_{42} (Wolfe *et al.*, 1999; Singleton *et al.*, 2000; Tanzi *et al.*, 2004; Shen and Kelleher, 2007). Additionally, the apolipoprotein E (*APOE*) ε3/4 allele is a major risk factor for sporadic Alzheimer's disease and is closely associated with late onset of disease and increased amyloid plaques in Alzheimer's disease (Reiman *et al.*, 1996; Mayeux *et al.*, 1998; Teasdale *et al.*, 2005; Koffie *et al.*, 2012). The aggregates of amyloid-β_{42} are a major component of senile plaques, affecting the formation of neurofibrillary tangles and consequently neuronal loss (Glenner *et al.*, 1984). Despite this fundamental understanding of Alzheimer's disease pathology, a lack of access to appropriate human neurons for modelling Alzheimer's disease remains a major challenge for moving therapeutic development forward.

Recent advances in direct reprogramming have garnered considerable interest for human disease modelling and cell replacement strategies (Vierbuchen and Wernig, 2011). Several studies have demonstrated the feasibility of generating human induced pluripotent stem cells from patients with rare, early-onset familial Alzheimer's disease mutations and sporadic Alzheimer's disease (Israel *et al.*, 2012; Kondo *et al.*, 2013; Young *et al.*, 2015; Raja *et al.*, 2016). However, the inefficient processes of induced pluripotent stem cell generation and directed differentiation into specific target cell populations limit the application of induced pluripotent stem cell technology in neurodegenerative disease modelling (HD iPSC Consortium, 2012; Arber *et al.*, 2015). More recently, several studies have reported the direct conversion of one specific somatic cell type to another by forced expression of master transcriptional regulators (Ieda *et al.*, 2010; Efe *et al.*, 2011; Marro *et al.*, 2011; Yang *et al.*, 2013). Pioneering work on neuronal reprogramming demonstrated the feasibility of direct conversion of mouse and human fibroblasts into functional neurons (Vierbuchen *et al.*, 2010), which can ultimately be applied to model neurological diseases and conduct drug screening against disease phenotypes more efficiently. Particularly, induced neuron-based modelling of late onset sporadic Alzheimer's disease would provide a useful approach to understanding sporadic Alzheimer's disease pathogenesis and facilitate therapeutic discovery.

Previously, we and others reported that both mouse and human fibroblasts can be directly converted into subtypes of functional neurons (Ambasudhan *et al.*, 2011; Kim *et al.*, 2011; Pfisterer *et al.*, 2011). Several lines of evidence suggested that the induced neurons display morphological and functional properties of neurons indicating that induced neurons can be used for neurological disease modelling (Cremades *et al.*, 2012; Meyer *et al.*, 2014). However, direct conversion into human induced neurons occurs with very low efficiency (Ambasudhan *et al.*, 2011; Pfisterer *et al.*, 2011). To overcome these challenges, we applied nanopattern topography to cultures of human induced neurons as an efficient stimulant for direct lineage reprogramming (Yoo *et al.*, 2015). We use this optimized lineage reprogramming system to demonstrate that induced neurons generating from sporadic patients with Alzheimer's disease harbouring *APOE* ε3/4 allele exhibit increased production of amyloid-β peptides. Moreover, these induced neurons recapitulate the pathological features and molecular signatures found in the primary neuronal tissue of *APOE* ε3/4 patients with Alzheimer's disease. We subsequently examined the transcriptional regulatory network in Alzheimer's disease induced neurons and identify the desmoglein 2 (*DSG2*) gene as a candidate modifier of the Alzheimer's disease phenotype. *DSG2* was previously found to be a risk factor for late onset Alzheimer's disease through genome-wide association studies (Lambert *et al.*, 2013; Karch and Goate, 2015). We thus tested the functional significance of *DSG2* dysregulation and observed that *DSG2* inhibition can suppress APOE ε3/4-induced neurotoxicity in both human and mouse induced neuron models. Taken together, our results demonstrate that induced neurons can be used to effectively model Alzheimer's disease and can provide a platform for the discovery and functional evaluation of candidate therapeutic modalities.

Materials and methods

Culture of mouse and human fibroblasts

Mouse embryonic fibroblasts were isolated from Tau-eGFP knock-in or wild-type embryonic Day 13 mouse embryos. After removing the head containing the spinal cord, dorsal root ganglia, and all internal organs, the remaining tissue was dissociated and incubated in trypsin (0.25%, Invitrogen) for 10–15 min. Single cells from each embryo were plated onto a 15 cm cell culture dish with mouse embryonic fibroblast medium [Dulbecco's modified Eagle medium (DMEM) containing 10% foetal bovine serum and 1% penicillin/streptomycin]. Human control (GM23967, male, condition: healthy control, *APOE* ε3/3 genotype) and Alzheimer's disease fibroblasts (AG11414, male, condition: Alzheimer's disease early

APOE ε3/4 genotype), (AG05810, female, condition: Alzheimer's disease *APOE* ε3/4 genotype), (AG05770, male, condition: unknown, *APOE* ε3/3 genotype), (AG06840, male, condition: Alzheimer's disease *PSEN1* mutation, *APOE* ε3/3 genotype), (AG09908, female, condition: Alzheimer's disease *PSEN2* mutation, *APOE* ε3/3 genotype) were purchased from the Coriell Cell Repository. Human fibroblasts were maintained in human fibroblast medium [DMEM containing 10% foetal bovine serum, 1% non-essential amino acid (Gibco), 0.1% β-mercaptoethanol (Gibco) and 1% penicillin/streptomycin (Gibco)].

Lentivirus generation and viral infection

To overexpress human *APOE* ε4 in mouse induced neurons, *APOE* ε4 cDNA from *APOE* ε3/4 patient fibroblasts was cloned into lentiplasmid and the lentivirus was infected with reprogramming factors. Lentivirus was produced in HEK293T cells, which were grown in DMEM containing 10% foetal bovine serum and 1% penicillin/streptomycin. Subsequently, the cells were transfected with the lentivirus construct, Ascl1, Brn2, Myt1l, NeuroD1, mutant APP, M2rtTA and psPAX2, pMD2.G vectors using calcium phosphate co-precipitation. Following transfection for ~24 h, the medium was changed and the viruses were harvested 48–72 h later. Mouse embryonic fibroblasts were infected with the lentivirus at passage 3, twice in 2 days. The infected mouse embryonic fibroblasts were cultured in N3 medium containing DMEM/F12, insulin (25 μg/ml), progesterone (20 nM), transferrin (50 μg/ml), putrescine (100 μM), laminin (1 μg/ml), basic fibroblast growth factor (25 μg/ml) and 1% penicillin/streptomycin.

Fabrication of nano-grooved substrates

Polyurethane acrylate nanoscale grooved patterns (300 nm ridge, groove width of 400 nm) were fabricated on glass substrates using UV-assisted capillary force lithography as previously described (Lee *et al.*, 2010; Yoo *et al.*, 2015). In brief, a UV curable polyurethane acrylate precursor solution (Minuta Tech. Inc.) was dispensed onto glass coverslips (diameter: 25 mm, thickness: 100 mm, Marienfeld) that had been coated with an adhesion promoter (phosphoric acrylate: isopropyl alcohol; 1:10 v/v). A flexible mould with nanoscale patterns was placed directly onto the surface, and the mould cavity was spontaneously filled with the polyurethane acrylate precursor via capillary action. The polyurethane acrylate nanoscale solution was cured by exposure to UV light (l ¼ 250 e400 nm) for ~30 s (100 mJ/cm^2) and the mould was peeled off using sharp tweezers. The as-synthesized nano-grooved substrates were cleaned using 70% ethanol, rinsed with distilled water and then coated with gelatin by immersion in a 0.1% (w/v) gelatin solution.

Direct conversion of human fibroblast into induced neurons

To generate human induced neurons, human fibroblasts were plated on nano-patterned substrates. Polybrene (Sigma) was used to improve the efficiency of the infection process. Plated human fibroblasts were infected with lentivirus FUW-Ascl1, Brn2, Myt1l, NeuroD1, Teto-mut APP, M2rtta three times in 2 days and were maintained in N3 medium containing DMEM/F12, insulin (25 μg/ml), progesterone (20 nM), transferrin (50 μg/ml), putrescine (100 μM), laminin (1 μg/ml), fibroblast growth factor basic (25 μg/ml), brain-derived neurotrophic factor (10 g/ml) and 1% penicillin/streptomycin. To overexpress mutant APP in induced neurons, doxycycline was treated at 7 days after initial factor infection.

Flow cytometry

Cells were dissociated using 0.125% trypsin-EDTA for 4 min and the single cells were then pelleted, resuspended in 4% paraformaldehyde, and incubated for 10 min at 4°C. Following this, the cells were washed with 1% bovine serum albumin twice, and resuspended in fluorescence-activated cell sorting buffer for analysis. Flow cytometry was performed using an Accuri instrument (Becton-Dickinson). All data were analysed with FlowJo vX software (TreeStar).

Immunofluorescent staining analysis

The cells were washed with phosphate-buffered saline (PBS) before being fixed in 4% paraformaldehyde in PBS. Cells were immunostained according to standard protocols using the following primary antibodies: Tuj1 (Sigma), MAP2 (Cell Signaling), VGluT1 (Abcam), NeuN (Millipore), Cleaved-caspase3 (Cell Signaling), Phosphorylated tau (AT8, Pierce), APP (Millipore), Nestin (Millipore), EEA1 (Millipore), Amyloid-β_{42} (Millipore) and appropriate fluorescent secondary antibodies (Invitrogen). Representative images were captured using a Nikon Eclipse Ti microscope. The directions, lengths and 3D features of the induced neurons were analysed using Adobe Photoshop® software.

Western blot analysis

Induced neurons were extracted using Tris-buffered saline (TBS) extraction buffer containing 1 × TBS buffer, 1 mM NaF, 1 mM $NaVO_3$, and protease inhibitor mixture (Roche) before being incubated on ice for 20 min. To obtain TBS-soluble fractions, the samples were centrifuged for 1 h at 20 000*g* at 4°C. The remaining pellets were then resuspended in 2% SDS extraction buffer containing 1 × TBS buffer, 1% Triton™ X-100, 2% SDS, 1 mM NaF, 1 mM $NaVO_3$, and protease inhibitor mixture (GenDepot) before being incubated on ice for 30 min. To obtain TBS-insoluble/SDS-soluble fractions, the samples were centrifuged for 1 h at 20 000*g* at 4°C. The supernatants were extracted and analysed to detect the protein levels. The TBS-insoluble/SDS-soluble fractions were electrophoresed on 12% Bis-Tris gels before being transferred to nitrocellulose membranes (GE Healthcare Biosciences). Representative images were captured using Chemidoc TRS+ with image lab software (Bio-Rad). The primary monoclonal antibodies were used as follows: anti-Beta-amyloid 6E10 (1:400, BioLegend), beta-actin (1:1000, Abfrontier).

Quantitative real-time polymerase chain reaction analysis

Quantitative real-time polymerase chain reaction (qRT-PCR) was performed using Platinum® SYBR® green qPCR SuperMix (Invitrogen). qRT-PCR analysis was conducted by the reverse transcription reaction in a Rotor-gene Q (QIAGEN). Total RNA was purified from the samples and isolated using an RNeasy® Kit (QIAGEN) according to the manufacturer's protocols. Gene expression of fibroblast and neuronal markers was normalized against GAPDH levels in each sample.

Amyloid-β ELISA

ELISA analysis was performed using a human amyloid-β assay ELISA kits (IBL). Neuronal culture media were collected from cultured induced neurons after 72–96 h before being centrifuged at 20 000*g* for min. To harvest intracellular amyloid-β_{40} and amyloid-β_{42}, cells were lysed by ELISA sampling buffer (1 × TBS buffer, 1% Triton™ X-100, 0.1% SDS). The collected samples were subjected to ELISA kits including amyloid-β (1–42) and amyloid-β (1–40), according to the manufacturer's instructions.

Electrophysiology

For electrophysiological analysis, cells were cultured on nanopatterned glass coverslips before being transferred to recording medium containing the extracellular solution [in mM: 130 NaCl, 4 KCl, 2 $CaCl_2$, 1 $MgCl_2$, 10 HEPES, 10 glucose (pH 7.35)]. Patch pipettes were filled with the intracellular solution (in mM: 110 potassium gluconate, 20 KCl, 2 Mg-ATP, 10 sodium phosphocreatine, 1.0 EGTA, 0.3 GTP-Tris, and 20 HEPES) (pH 7.25). Electrodes were fabricated from borosilicate capillary glass tubing (Warner Instruments) with a capillary glass puller (Sutter Instruments). The patch electrodes were fire-polished using a microforge (Narishige) and had resistances of 2–4 MΩ. After establishing whole-cell mode, the cell membrane capacitance, and series resistance were compensated to 75% electronically using a patch clamp amplifier (Axopatch 200B; Molecular Devices). Data generation and acquisition were performed using the pClamp10 software on an IBM computer equipped with an analogue-to-digital converter (Digidata 1440 A; Axon Instruments). Once current-clamp mode was obtained, the cell was maintained at a potential of approximately −65 to −70 mV. Current injection protocol steps were applied ranging from −100 pA to +120 pA. Inward sodium current and outward potassium current were measured in voltage-clamp mode with voltage step protocols ranging from −55 to +55 mV.

Gene expression profiling, gene set enrichment analysis, and network analysis

Affymetrix GeneChip Human Gene 2.0 ST Array was performed according to the manufacturer's protocol. Robust Multiarray Averaging method using affy R package was used for normalization and summarization. When multiple probes were available, averaged values per gene were applied. Gene set enrichment analysis (Subramanian *et al.*, 2005) was performed using gene set enrichment analysis pre-ranked mode to determine whether gene sets were statistically enriched in both *APOE* ε3/4 sporadic Alzheimer's disease patient induced neurons versus *APOE* ε3/3 control induced neurons and *APOE* ε3/4 sporadic Alzheimer's disease patient versus *APOE* ε3/3 controls in human brain tissue (GSE48350). Curated gene sets (1691 genes of BLALOCK_ALZHEIMERS_DISEASE and 390 genes of BLALOCK _ALZHEIMERS_DISEASE_INCIPIENT) in Molecular Signatures Database v5.1 and differentially expressed genes (fold change ⩾ 2) in *APOE* ε3/4 patient induced neurons versus *APOE* ε3/3 control induced neurons were used. The results of gene set enrichment analysis are considered significant when the false discovery rate and nominal *P*-value are < 0.05. The interactome of proteins in *Homo sapiens* was obtained from NCBI Gene (ftp://ftp.ncbi.nlm.nih.gov/gene/GeneRIF/). To identify the gene network found in Alzheimer's disease patients with *APOE* ε3/4 genotype-derived induced neurons, the protein-protein interactions among differentially expressed genes were imported into Cytoscape (http://www.Cytoscape.org, v3.3.0) (Shannon *et al.*, 2003) and analysed using Molecular Complex Detection, v1.4.1 (Bader and Hogue, 2003) to find the protein network modules. The data supporting the findings of this study are available in the Supplementary material or from the corresponding author on request.

Statistical analysis

All data are presented as the mean ± standard deviation (SD) of three independent experiments. *n*-Values indicate the number of independent experiments performed or the number of individual experiments or mouse. For each independent *in vitro* experiment, at least three technical replicates were used and a minimum number of three independent experiments were performed to ensure adequate statistical power. In all of the analyses, group differences were considered statistically significant at $P < 0.05$. ($^*P < 0.05$, $^{**}P < 0.01$). ANOVA test was used for multi-component comparisons and Student's *t*-test for two-component comparisons after the normal distribution was confirmed.

Results

Alzheimer's disease modelling in mouse induced neurons

In proof-of-principle studies, we initially established induced neurons from mouse fibroblasts to model Alzheimer's disease pathology. To develop mouse induced neurons that produce a high level of toxic amyloid-β, we overexpressed a human APP containing 670/M671 Swedish mutations. First, mouse fibroblasts were transduced with lentivirus constitutively expressing Ascl1, Brn2, and Myt1l along with a doxycycline-inducible mutant APP lentivirus (Fig. 1A). Seven days of Ascl1, Brn2, Myt1l expression was previously shown to be sufficient for converting mouse fibroblasts into functional induced neurons (Vierbuchen

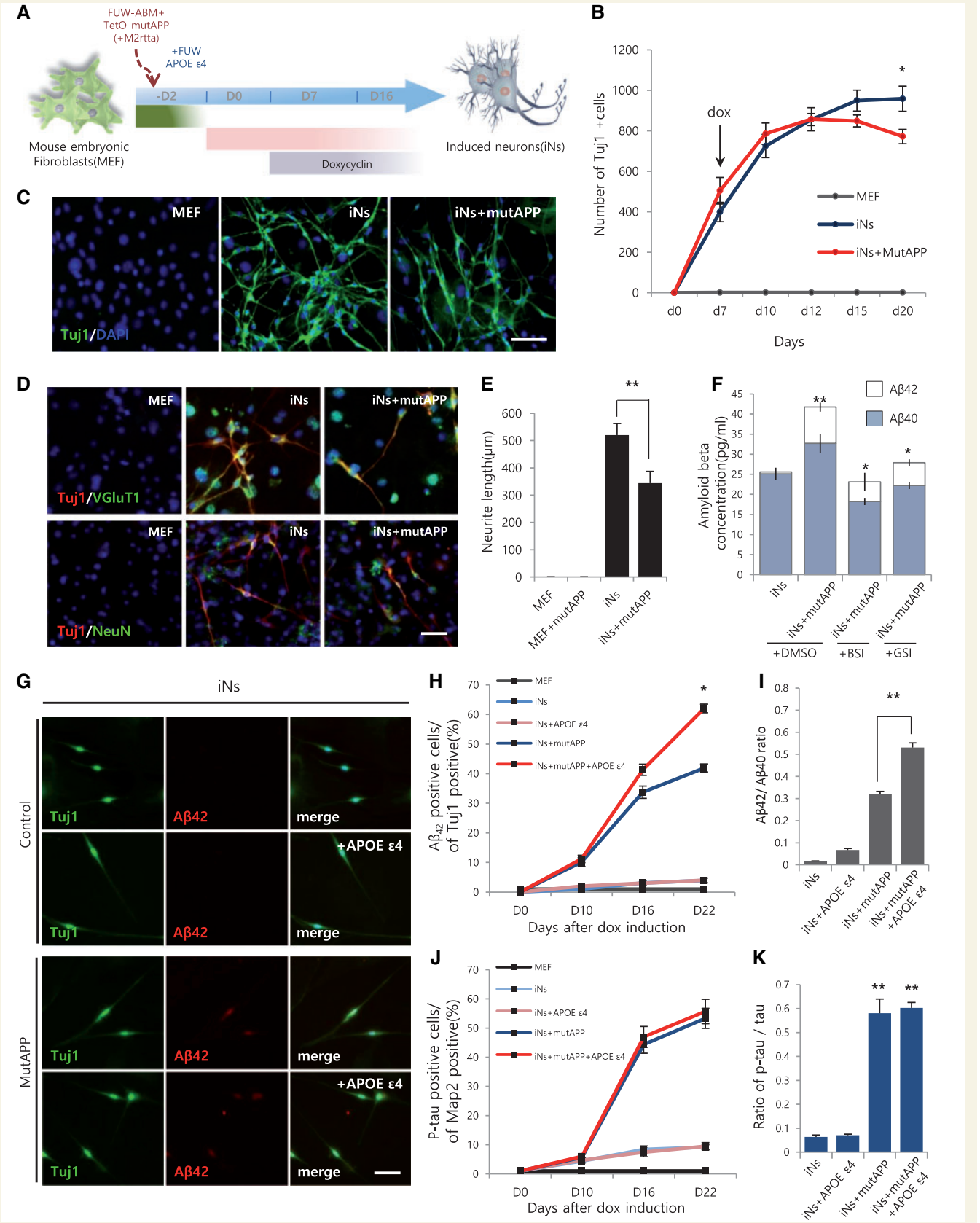

Figure 1 Modelling Alzheimer's disease phenotypes in mouse induced neurons. (**A**) Schematic of modelling Alzheimer's disease (AD) phenotypes in mouse induced neurons (iNs). Mouse embryonic fibroblasts (MEFs) were transduced with lentivirus constitutively expressing Ascl1, Brn2, and Myt1l along with a doxycycline-inducible human mutant *APP* lentivirus and FUW-APOE ε4 lentivirus. To induce Alzheimer's disease phenotypes in the reprogrammed induced neurons, doxycycline was introduced into the culture 7 days after initial Ascl1, Brn2, and Myt1l induction. (**B**) The number of

(continued)

et al., 2010). We also confirmed that at Day 7, prior to doxycycline-induction, there was no distinction between the control FUW-Ascl1, Brn2, and Myt1l infected cultures and those also containing the doxycycline-inducible APP (Fig. 1B and Supplementary Fig. 1A–D). To avoid the effects of mutant APP on the formation induced neurons, doxycycline was introduced into the culture 7 days after Ascl1, Brn2, Myt1l expression (Fig. 1A). Fifteen days after Ascl1, Brn2, Myt1l expression, control induced neurons exhibited expression of neuronal markers such as Tuj1, VGluT1 and NeuN (Fig. 1C and D), which were not observed in fibroblasts transduced with control lentivirus (Fig. 1C and D, left panel). Consistent with previous reports, we observed that most Tuj1-positive mouse induced neurons were also positive for the glutamatergic neuron marker, VGluT1 and the mature post-mitotic neuron marker, NeuN (Fig. 1C and D, and Supplementary Fig. 1E). However, we were not able to observe expression of markers of neural progenitor/stem cells such as Nestin (Supplementary Fig. 1F), suggesting these induced neurons more closely resemble mature glutamatergic forebrain neurons.

Remarkably, we observed that the induced neuron cultures overexpressing human mutant APP exhibited decreased neurite length and numbers of neuronal specific Tuj1-, VGluT1- and NeuN-positive cells (Figure 1B, D, E and Supplementary Fig. 1E). We also examined the number of Tuj1+ induced neurons in the cultures across different time points, and found that 8 days of APP induction resulted in a significant decrease in the number of Tuj1+ cells (Fig. 1B and Supplementary Fig. 1B), suggesting that mutant APP expression may lead to degeneration of the induced neurons. Consist with these results, expression of neuronal transcripts *Mapt*, *Map2*, *Gad1* (GAD67), *Tbr1*, *Syn1*, and *Bcl11b* (Ctip2), were all markedly decreased in APP expressing induced neuron cultures relative to controls (Supplementary Fig. 1G). Additionally, induced neurons derived from Tau-eGFP fibroblasts were ~7% GFP+, and the frequency of Tau-eGFP+ induced neurons was significantly decreased in APP-expressing cultures (Supplementary Fig. 1H).

As a proof of the utility of mouse induced neurons in Alzheimer's disease modelling, we first examined Alzheimer's disease-associated phenotypes in APP expressing induced neuron cultures. Immunocytochemical analysis conducted 8 days after APP induction revealed that most APP-expressing induced neurons express amyloid-β_{42} (Fig. 1G). We monitored the number of amyloid-β_{42}+/Tuj1+ cells over a period of 3 weeks from the onset of doxycycline induction and observed a rapid, linear increase in amyloid-β_{42}+ and Tuj1+ double-positive neurons across the time course, but APP expressing induced neurons exhibited the most significant increase in amyloid-β_{42}+ neurons (Fig. 1H). Amyloid-β_{42} is a major component of amyloid plaques found in the brains of patients with Alzheimer's disease, and an increased amyloid-β_{42}:amyloid-β_{40} ratio is a key feature of Alzheimer's disease pathogenesis (Serneels *et al.*, 2009). Thus, we examined extracellular amyloid-β secretion in the mutant APP-expressing mouse induced neurons. Importantly, we observed increased amyloid-β_{42} secretion into the medium of APP-expressing induced neurons and a significantly elevated amyloid-β_{42}:amyloid-β_{40} ratio compared with control and APP only expressing induced neurons (Fig. 1I). Hyperphosphorylation and abnormal accumulation of the microtubule-associated protein tau (MAPT) are key pathological features of Alzheimer's disease (Gotz *et al.*, 1995; Shi *et al.*, 2012). Detection of tau phosphorylation, Ser202 and Thr205 with the AT8 antibody revealed increased p-tau accumulation in APP expressing induced neurons (Fig. 1J). Moreover, we observed co-staining of p-tau with MAP2, and the ratio of p-tau/tau was significantly increased in APP expressing induced neurons, suggesting that phosphorylated tau was aberrantly localized in these cells (Fig. 1J and K).

APP is largely processed in the vesicular endosomal compartments, and increased APP expression leads to alterations of intracellular trafficking, which has consequently been implicated in Alzheimer's disease pathogenesis (Thinakaran and Koo, 2008). Thus, we examined whether APP-expressing induced neurons exhibit abnormal APP localization in vesicular endosomal compartments. We observed that localization of APP puncta positive for an

Figure 1 Continued

Tuj1+ cells in fibroblasts, induced neurons and APP-expressing induced neurons at different time points. To induced mutant APP expression, doxycycline was treated on Day 7 after initial factor infection. Data represent mean ± SEM. Student's *t*-test, $^*P < 0.05$, $^{**}P < 0.01$; $n = 4$ per each sample. (**C**) Immunofluorescence of Tuj1+ induced neurons in the presence and absence of mutant APP induction for 8 days. Scale bar = 100 μm. (**D**) Co-staining of induced neuron cultures with the Tuj1, VGluT1 and NeuN at 8 days after doxycycline induction. Scale bar = 100 μm. (**E**) Measurement of the neurite length of control and APP expressing induced neurons. Data represent mean ± SEM. Student's *t*-test, $^{**}P < 0.01$; $n = 5$ per each sample. (**F**) ELISA analysis of amyloid-β_{42} (*top*) and amyloid-β_{40} (*bottom*) secreted from controls and APP expressing induced neurons treated with β-secretase inhibitor and γ-secretase inhibitor. Data represent mean ± SEM. ANOVA test, $^*P < 0.05$, $^{**}P < 0.01$; $n = 6$ per each sample. (**G**) Immunofluorescence staining showing the production of amyloid-β_{42} on 16 days after doxycycline induction. Scale bar = 100 μm. (**H**) The number of amyloid-β_{42} positive cells per Tuj1+ at different time point after doxycycline induction. Data represent mean ± SEM. ANOVA test, $^*P < 0.05$, $^{**}P < 0.01$; $n = 6$ per each sample. (**I**) The ratio of amyloid-β_{42}/amyloid-β_{40} in control, APP expressing induced neurons and APP expressing APOE ε4/4 induced neurons at 16 days after doxycycline induction. Data represent mean ± SEM. Student's *t*-test, $^{**}P < 0.01$; $n = 6$ per each sample. (**J**) The number of phosphorylated tau/Map2-positive cells after doxycycline induction. Data represent mean ± SEM. $n = 3$ per each sample. (**K**) The ratio of p-tau/total tau in control, APP expressing induced neurons and *APP* and human *APOE* ε4 expressing induced neurons. Data represent mean ± SEM. ANOVA test, $^*P < 0.05$, $^{**}P < 0.01$; $n = 6$ per each sample. Dox = doxycycline.

early endosomal marker, EEA1, in induced neurons, and the number of APP/EEA1 double positive compartments was significantly increased in mutant APP-expressing induced neurons (Supplementary Fig. 2A and B), whereas no differences in the expression of the APP processing enzyme β-secretase-1 (BACE1) were observed (Supplementary Fig. 2C).

Next, we examine the susceptibility of APP-expressing induced neurons to hydrogen peroxide-induced oxidative damage. Eight days after doxycycline induction, APP-expressing induced neurons were treated with the various concentrations of hydrogen peroxide for 24 h and cells were fixed and stained for Tuj1 and cleaved caspase-3. We observed a decrease in the frequency of Tuj1+ cells and a concomitant increase in cleaved caspase-3+ apoptotic induced neurons upon APP overexpression at all concentrations of hydrogen peroxide (Supplementary Fig. 2D–F). Taken together, these data suggest that mouse induced neurons can faithfully recapitulate Alzheimer's disease phenotypes at least in part as evidenced by the accumulation of amyloid-β_{42}, tau phosphorylation, abnormal endocytic function and susceptibility to oxidative stress-induced cell death. To examine whether APP-expressing induced neurons represent a tractable model for evaluating therapeutic candidates, we further assessed their response to pharmacological inhibition of the γ- and β-secretase complexes, which sequentially cleave APP into amyloid-β species. Indeed, inhibition of γ- and β-secretase complexes in APP-expressing induced neuron cultures significantly attenuated secretion of both amyloid-β_{42} and amyloid-β_{40}, as well as the extracellular accumulation of amyloid-β_{42} (Fig. 1F and Supplementary Fig. 2G and H). Furthermore, the expression of neuronal marker genes, *Map2*, *Neurod1*, *Syn1*, and *Gad1* (GAD67) was partially restored in APP-expressing induced neurons treated with β-secretase inhibitors (Supplementary Fig. 2I). In addition, we observed that APP expression led to thioflavin T-positive deposits, and these deposits were significantly decreased by treatment with β-secretase inhibitors (Supplementary Fig. 2J–L), demonstrating that this model system can be used for testing therapeutic strategies against Alzheimer's disease, as previously suggested (Frackowiak *et al.*, 2003; Choi *et al.*, 2014; Muratore *et al.*, 2014).

Additionally, to determine whether the expression of the late onset Alzheimer's disease risk factor *APOE* ε4 allele can directly affect APP processing and amyloid-β_{42} generation in induced neurons, we next assessed the number of amyloid-β_{42}+ cells and the ratio of amyloid-$\beta_{42/40}$ in human *APOE* ε4-expressing mouse induced neurons (Fig. 1G–I). Importantly, we observed that APP/APOE ε4-expressing cultures had significantly increased numbers of amyloid-β_{42} positive induced neurons and extracellular accumulation of amyloid-β_{42} (Fig. 1G and H). Taken together, these results indicate that mouse induced neurons expressing mutant APP and/or APOE ε4 can represent a valid model for studying APOE ε4-associated sporadic Alzheimer's disease pathogenesis and screening for potential therapeutics.

Modelling *APOE* ε3/4-associated sporadic Alzheimer's disease in human induced neurons

Human induced neurons can be derived from fibroblasts using a specific combination of transcription factors (Vierbuchen *et al.*, 2010; Ambasudhan *et al.*, 2011; Pfisterer *et al.*, 2011). We initially attempted to reprogram human fibroblasts into induced neurons using the previously reported factor combination *ASCL1*, *BRN2*, *MYT1L* and *NEUROD1*. However, in our laboratory, this combination of reprogramming factors leads to the inefficient generation of TUJ1+ human induced neurons, precluding the type of analysis performed on murine induced neurons presented above (Fig. 2A and B). Thus, we reasoned that additional variables need to be modified along with reprogramming factor expression in order to enhance the efficiency of generating human induced neurons. Recent evidence indicates that cell fate determination can be influenced by modulating biophysical cues such as surface nano-topography (Ravichandran *et al.*, 2009; Pan *et al.*, 2013; Solanki *et al.*, 2013), and we previously found that nanoscale biophysical stimulation by nanopatterned substrates promotes highly efficient direct lineage reprogramming of mouse fibroblasts into induced functional neurons (Yoo *et al.*, 2015). Thus, we examined whether human fibroblasts also can be more efficiently reprogrammed into the neuronal state using nano-topography, and subsequently whether resulting cells could serve as a model for human Alzheimer's disease. To determine whether nano-topographical cues, when combined with ectopic factor expression, can improve reprogramming efficiency, we plated *ASCL1*, *BRN2*, *MYT1L* and *NEUROD1*-infected human fibroblasts on nano-grooved substrates, which were fabricated with a 400 nm groove width separated by 300 nm ridges (Supplementary Fig. 3A and B). Consistent with previous reports, reprogramming human fibroblasts on nanopatterned substrates resulted in apparent changes in cell alignment and elongation along the patterned surface (Supplementary Fig. 3C and F). In this context, direct lineage reprogramming on the nanopatterned substrates resulted in a greater number of cells taking on neuronal morphology and TUJ1 expression relative to non-patterned surfaces (Fig. 2A).

Seven days after factor infection, doxycycline induction of the mutant APP lentivirus was used as in the murine system described above. Human induced neurons on the nanopatterned surface expressing mutant APP exhibited decreased TUJ1+ cell numbers relative to control human induced neurons (Fig. 2A and B). Importantly, in the absence of nanopatterning, these differences could not be observed due to the baseline inefficiency of the human induced neuron conversion, highlighting the importance

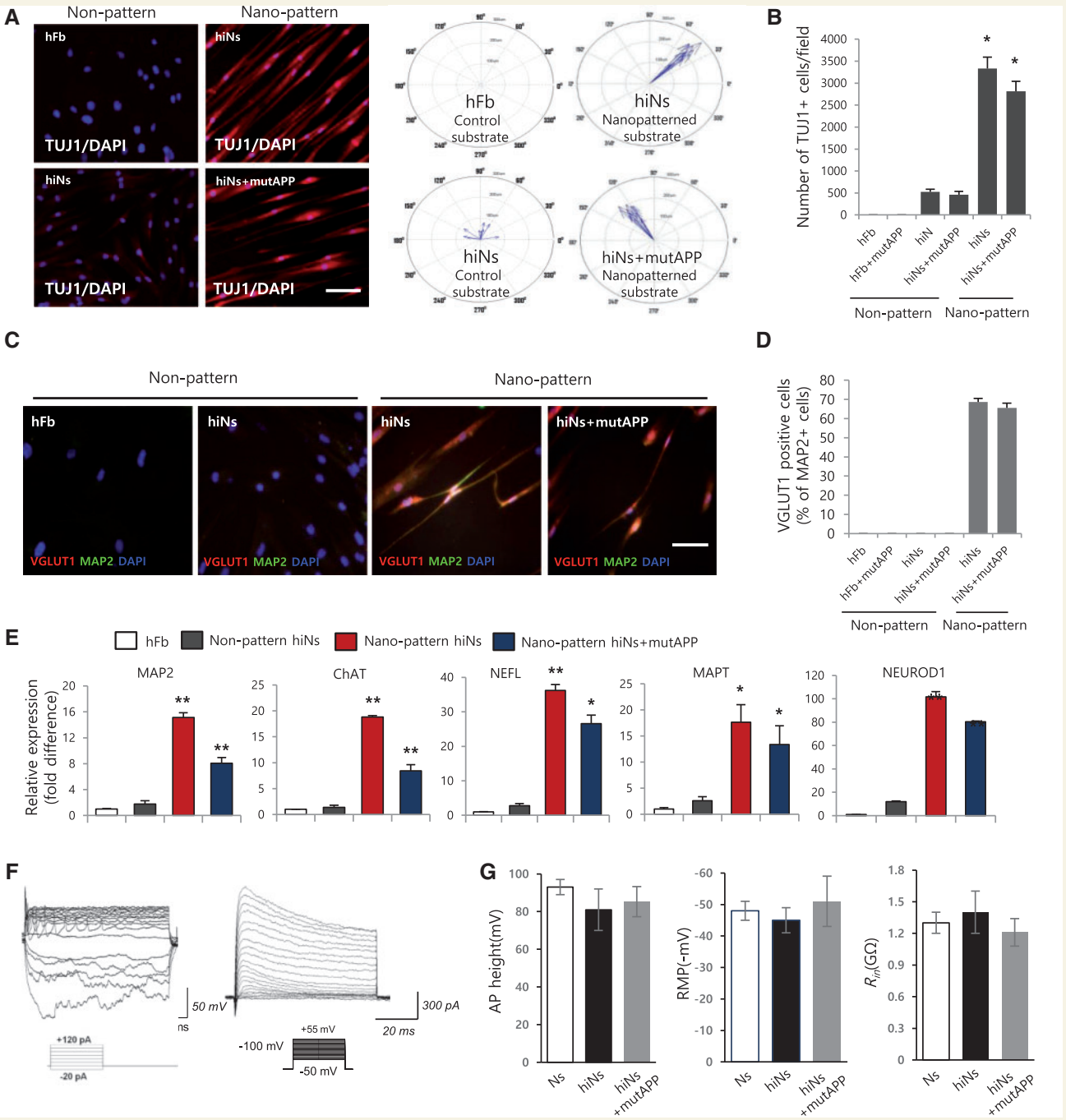

Figure 2 Efficient direct lineage conversion of human fibroblasts into human induced neurons on nanopatterned substrates. (**A**) Representative immunostaining showing the expression of TUJ1 (*left*) and compass plots (*right*) of *ASCL1*, *BRN2*, *MYT1L* and *NEUROD1* derived human induced neurons (hiNs) on a non-patterned and a nanopatterned substrates in the absence and presence of APP expression. Scale bar = 100 μm. (**B**) The number of TUJ1+ human induced neurons on control and a nanopatterned substrates in the absence and presence of APP overexpression. Data represent mean ± SEM. ANOVA test, $*P < 0.05$; $n = 6$ per each sample. (**C**) The images show the MAP2 and VGLUT1 positive human induced neurons and APP expressing human induced neurons on the control and nanopatterned substrates at 8 days after doxycycline induction. Scale bar = 100 μm. (**D**) The percentage of VGLUT1/MAP2-positive cells on 8 days after doxycycline induction. Data represent mean ± SEM. (**E**) qRT-PCR analysis of neuronal markers (*MAP2*, *CHAT*, *NEFL*, and *MAPT*) at 8 days after doxycycline induction. Data represent mean ± SEM. ANOVA test, $*P < 0.05$, $**P < 0.01$; $n = 3$ per each sample. (**F**) Action potentials and sodium and potassium currents of human induced neurons and APP expressing human induced neurons on the nanopatterned substrates. $n = 14$ each group (**G**) Electrophysiological analysis of human induced neurons and APP expressing human induced neurons on the nanopatterned substrates. Data represent mean ± SEM, $n = 12$ each group. hFb = human fibroblasts.

of efficiently reprogrammed cultures for Alzheimer's disease modelling (Fig. 2A and B). Consistent with the increased number of human induced neurons generated, immunocytochemistry conducted 15 days after reprogramming revealed that the nanopatterned substrates enable the expression of mature neuronal markers including MAP2 and VGLUT1 (Fig. 2C and D). Culture on nanopatterned substrates significantly increased the expression of pan-neuronal marker genes including *MAP2*, *CHAT*, *NEFL*, *MAPT* and the endogenous *NEUROD1*, and this expression was attenuated by induction of mutant APP (Fig. 2E). Additionally, to examine the reprogramming efficiency of human fibroblasts, we counted red fluorescent protein positive cells derived from cultures harbouring a synapsin-red fluorescent protein reporter by flow cytometry. Reprogramming for 15 days on nanopatterned substrates resulted in a 3-fold increase in the number of synapsin-red fluorescent protein positive human induced neurons, relative to control (Supplementary Fig. 3D). Next, we evaluated the morphological characteristics of control and *APP*-expressing induced neurons on nanopatterned substrates. Eight days after doxycycline induction, human fibroblasts developed into induced neurons with typical neuronal morphology, including dramatically decreased soma size and increased neurite length (Supplementary Fig. 3E). Importantly, we did not observe decreased soma size in *APP*-expressing induced neurons, and observed a decrease in neurite length on the nanopatterned substrates (Supplementary Fig. 3E). Electrophysiological recordings showed that both the control induced neurons and *APP*-expressing induced neurons (14 cells each group) cultured on nanopatterned substrates elicit action potentials as well as sodium and potassium currents (Fig. 2F). Electrophysiological characteristics of human induced neurons on nanopatterned substrates including resting membrane potential, input resistance, and action potential amplitude indicates that these cells are highly functionally similar to *bona fide* primary neurons (Fig. 2G). Taken together, these data indicate that human induced neurons on nanopatterned substrates exhibit well developed and functional neuronal characteristics, and *APP*-expressing human induced neurons can be used for Alzheimer's disease modelling.

Next, we applied our human induced neuron conversion protocol to fibroblasts derived patients with sporadic forms of Alzheimer's disease and examined sporadic Alzheimer's disease-associated pathology in these induced neurons. We prepared human fibroblasts from both healthy control in *APOE* ε3/3 isoform genotype and sporadic Alzheimer's disease patient harbouring an Arg112 and Arg158 in *APOE* ε3/4 isoform genotype (Patient AG11414). This *APOE* ε3/4 allele is a major risk factor for sporadic Alzheimer's disease and is associated with earlier onset of Alzheimer's disease and increased amyloid plaques (Kim *et al.*, 2009; Duan *et al.*, 2014).

As in previous experiments, we induced reprogramming of sporadic Alzheimer's disease patient fibroblasts on the nanopatterned substrates after infection. The human induced neuron cultures on nanopatterned substrates aligned with groove direction and exhibited an increase in neuronal morphology and reprogramming efficiency assessed by the per cent of TUJ1+ and MAP2+ cells (Supplementary Fig. 3F and G). We did not observe significant differences in the number of TUJ1+/MAP2+ induced neurons between control (*APOE* ε3/3 allele) and patient (*APOE* ε3/4 allele)-derived cultures (Supplementary Fig. 3F and G). In addition, we did not observe significant changes in the number of TUJ1+ cells in long-term cultures (40 days, data not shown), suggesting that *APOE* ε3/4 patient induced neurons do not exhibit the Alzheimer's disease-associated degeneration in culture in the absence of other perturbation. However, we did observe a modest decrease in the number of TUJ1+/MAP2+ induced neurons in APP-expressing *APOE* ε3/4 patient induced neurons (Supplementary Fig. 3F and G). Remarkably, sporadic Alzheimer's disease patient induced neurons and APP-expressing induced neurons cultured on nanopatterned substrates exhibited accumulation of amyloid-β polymers (Fig. 3A), suggesting that efficient reprogramming of *APOE* ε3/4 Alzheimer's disease patient induced neurons on the nanopatterned substrates is critical for the generation of Alzheimer's disease phenotypes in the induced neurons. Moreover, APP-expressing *APOE* ε3/4 patient induced neurons show a greater accumulation of amyloid-β polymers (Fig. 3A), demonstrating this system can be used as a model for Alzheimer's disease. Additionally, we observed significant increases in amyloid-β_{42}-positive cells and tau phosphorylation in both APP-expressing *APOE* ε3/3 human induced neurons and *APOE* ε3/4 patient induced neurons 10 days after doxycycline induction (Fig. 3B, D and E). Furthermore, the expression of neuronal genes was significantly decreased in mutant APP-expressing *APOE* ε3/4 patient induced neurons on nanopatterned substrates (Fig. 3C).

Consistent with these results, localization of APP-positive puncta in early endosomes was significantly increased in APP-expressing patient induced neurons as confirmed by containing with early endosome associated antigen-1, EEA1 (Supplementary Fig. 4A and B). As expected, *BACE1* transcript levels were upregulated in nanopattern-derived patient induced neurons (Supplementary Fig. 4C), but did not appear altered upon mutant APP expression (data not shown), suggesting that the abnormal accumulation of amyloid-β_{42} in patient induced neurons is not caused by increased activity of *BACE1*. Additionally, we examined the pharmacological response to inhibitors in these patient induced neurons. Eight days after doxycycline induction, patient induced neurons were treated by γ- and β-secretase inhibitors. Consistent with results in murine cultures, inhibition of γ- and β-secretase complexes significantly attenuated the number of amyloid-β_{42} positive cells in the APP-expressing patient induced neurons (Fig. 3F, Supplementary Fig. 4D and E). Finally, we tested for susceptibility of APP-expressing patient induced neurons to

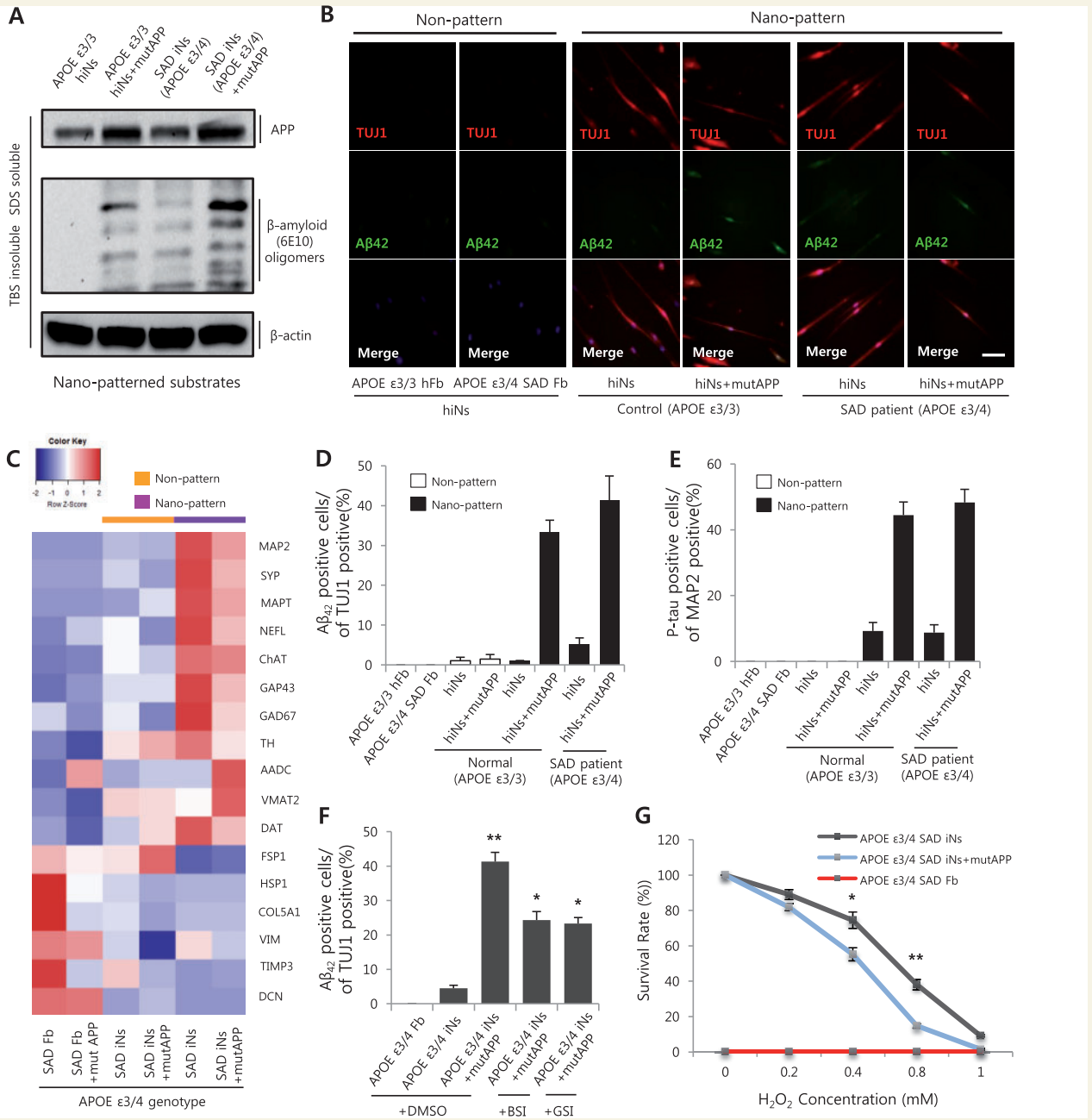

Figure 3 Pathological analysis of *APOE* ε3/4 patient induced neurons on a nanopatterned substrate. (**A**) Western blot analysis shows increase of amyloid-β oligomers in normal human fibroblasts and *APOE* ε3/4 patient, and APP expressing human induced neurons on nanopatterned substrates at 10 days after doxycycline induction. (**B**) Immunostaining of TUJ1 and amyloid-β_{42} in the no intracellular amyloid-β_{42} accumulation in human induced neurons on non-pattern, normal human fibroblasts (*APOE* ε3/3 genotype) and sporadic Alzheimer's disease patient (*APOE* ε3/4 genotype) derived human induced neurons on nanopatterned substrates. Scale bar = 100 μm. (**C**) Expression profiling using qRT-PCR analysis of patient fibroblasts, APP expressing fibroblasts, *APOE* ε3/4 patient induced neurons, APP expressing *APOE* ε3/4 patient induced neurons on the control (yellow) and nanopatterned (purple) substrates. Ratios of expression differences are shown in different colours. Red and blue represent higher and lower gene expression levels; $n = 6$ per each sample. (**D**) The percentage of amyloid-β_{42}/TUJ1 positive *APOE* ε3/4 patient human induced neurons 10 days after doxycycline induction. Data represent mean ± SEM. (**E**) The percentage of p-tau/MAP2-positive *APOE* ε3/4 patient human induced neurons on 10 days after doxycycline induction. Data represent mean ± SEM. (**F**) Decrease in amyloid-β_{42} + /TUJ1 positive APOE ε3/4 patient induced neurons and APP expressing *APOE* ε3/4 patient induced neurons on a nano-grooved pattern by β-secretase inhibitor and γ-secretase inhibitor treatment. Data represent mean ± SEM. ANOVA test, $^*P < 0.05$, $^{**}P < 0.01$; $n = 6$ per each sample. (**G**) Survival rate of hydrogen peroxide treated *APOE* ε3/4 patient fibroblasts, *APOE* ε3/4 patient induced neurons, APP expressing APOE ε3/4 patient induced neurons on nanopatterned substrates. Data represent mean ± SEM. Student's *t*-test, $^*P < 0.05$, $^{**}P < 0.01$; $n = 6$ per each sample.
SAD = sporadic Alzheimer's disease.

hydrogen peroxide. Patient induced neurons were treated with 0–1.0 mM of hydrogen peroxide and survival was evaluated after 24 h. *APOE* ε3/4 patient induced neurons progressively degenerated within 24 h at 0.2–1.0 mM, and APP-overexpressing *APOE* ε3/4 patient induced neurons were more susceptible to peroxide-induced cell death (Fig. 3G). Taken together, these results suggest that APOE ε3/4 Alzheimer's disease patient-derived induced neurons represent a valid model for studying sporadic Alzheimer's disease pathogenesis, and provide a novel strategy of screening of candidate therapeutics.

Next, to gain insight into the molecular mechanism of *APOE* ε3/4-associated sporadic Alzheimer's disease pathologies in induced neurons, we compared the global gene expression profiles of *APOE* ε3/3 healthy control and *APOE* ε3/4 patient-derived induced neurons in the presence and absence of APP expression. *APOE* ε3/4 sporadic Alzheimer's disease patient induced neurons expressing mutant APP exhibited dramatic changes in global gene expression (Fig. 4A). We found that 1500 genes were upregulated in the APOE ε3/4 Alzheimer's disease patient induced neurons, and 1298 genes were upregulated in APP-expressing *APOE* ε3/4 patient induced neurons compared to control *APOE* ε3/3 induced neurons (Fig. 4A and Supplementary Fig. 5A), whereas 1015 and 1383 genes were downregulated in the *APOE* ε3/4 patient induced neurons, and APP-expressing *APOE* ε3/4 patient induced neurons relative to control *APOE* ε3/3 induced neurons, respectively (Fig. 4A and Supplementary Fig. 5A). We also found that 314 upregulated and 196 downregulated genes were common between *APOE* ε 3/4 patient induced neurons and APP-expressing *APOE* ε3/4 patient induced neurons, indicating these are specific genes affected by the *APOE* ε3/4 genotypes (Fig. 4A and Supplementary Fig. 5A).

Additionally, when the distribution of expression changes of all genes was compared, we found that the expression patterns of human *APOE* ε3/4 induced neurons was significantly different from control *APOE* ε3/3 induced neurons, and that the changes in gene expression induced by mutant APP expression were not as significant as those conferred by the *APOE* ε3/4 genotype (Fig. 4B). Moreover, among the differentially expressed genes in APOE ε3/4 induced neuron cultures were genes known to be associated with APP processing including *BACE2*, *CLU*, *DSG2*, *PLAU* and *MME* (Fig. 4C), suggesting that the differential expression patterns of these genes may be associated with the development of *APOE* ε3/4-associated sporadic Alzheimer's disease.

Next, to examine the extent to which *APOE* ε3/4 sporadic Alzheimer's disease patient-derived induced neurons molecularly resemble primary patient neurons, we compared gene expression patterns between *APOE* ε3/4 Alzheimer's disease induced neurons and *APOE* ε3/4 Alzheimer's disease patient post-mortem brain (Curated gene sets in Molecular Signatures Database, MSigDB v5.1). Remarkably, gene set enrichment analysis indicates upregulated genes in *APOE* ε3/4 Alzheimer's disease patient induced neurons relative to control *APOE* ε3/3 induced neurons were enriched in primary incipient *APOE* ε3/4 Alzheimer's disease patient brain tissue (Fig. 4D, left) and *APOE* ε3/4 Alzheimer's disease patient brain tissue gene sets (Fig. 4D, right). Moreover, genes differentially expressed in the *APOE* ε3/4 Alzheimer's disease patient post-central gyrus were significantly enriched for differentially expressed genes from *APOE* ε3/4 induced neurons versus control *APOE* ε3/3 induced neurons (Fig. 4E, left) as well as for the genes whose differential expression was common between *APOE* ε3/4 induced neurons and APP-expressing *APOE* ε3/4 induced neurons (Fig. 4E, right), suggesting that *APOE* ε3/4 Alzheimer's disease patient-derived induced neurons faithfully recapitulates the molecular pathology in *APOE* ε3/4-associated sporadic Alzheimer's disease.

To gain insight into the molecular mechanism by which the *APOE* ε3/4 genotype promotes the development of sporadic Alzheimer's disease, we combined the differentially expressed genes between *APOE* ε3/4 patient induced neurons and control *APOE* ε3/3 induced neurons with the human protein-protein interaction HTRIdb database and analysed networks with *APOE* ε3/4 specific genes (Fig. 5A and Supplementary Fig. 5B). The target nodes and edges of networks are depicted with the proteins encoded by differential expressed genes and their interactions. Surprisingly, we found that the major sub-network from the highest molecular complex detection analysis was a DSG2-associated complex (Fig. 5B, C and Supplementary Fig. 5C), which is a known Alzheimer's disease genetic risk factor (Karch and Goate, 2015). This network analysis suggests that DSG2 may be functionally important in the development of *APOE* ε3/4-associated sporadic Alzheimer's disease.

To investigate the functional role of DSG2 in *APOE* ε3/4-associated sporadic Alzheimer's disease further, we initially confirmed the differential expression of *DSG2* using qRT-PCR and microarray-based transcriptome profiles. Remarkably, we found that *DSG2* was the most upregulated gene in *APOE* ε3/4 patient induced neurons and APP-expressing *APOE* ε3/4 patient induced neurons compared to control induced neurons with *APOE* ε3/3 genotype (Fig. 5D). Next, we prepared additional human fibroblasts from a control with APOE ε3/3 genotypes, familial patients with Alzheimer's disease with PSEN mutations, sporadic Alzheimer's disease with *APOE* ε3/4 genotypes, and idiopathic, sporadic Alzheimer's disease (Fig. 5E and Supplementary Fig. 5D). Interestingly, when human induced neurons were generated by *ASCL1*, *BRN2*, *MYT1L* and *NEUROD1* factor expression, *DSG2* was specifically upregulated in the induced neurons derived from sporadic Alzheimer's disease fibroblasts with *APOE* ε3/4 genotypes, relative to induced neurons derived from familial PSEN mutant fibroblasts, idiopathic sporadic Alzheimer's disease or controls with *APOE* ε3/3 genotype,

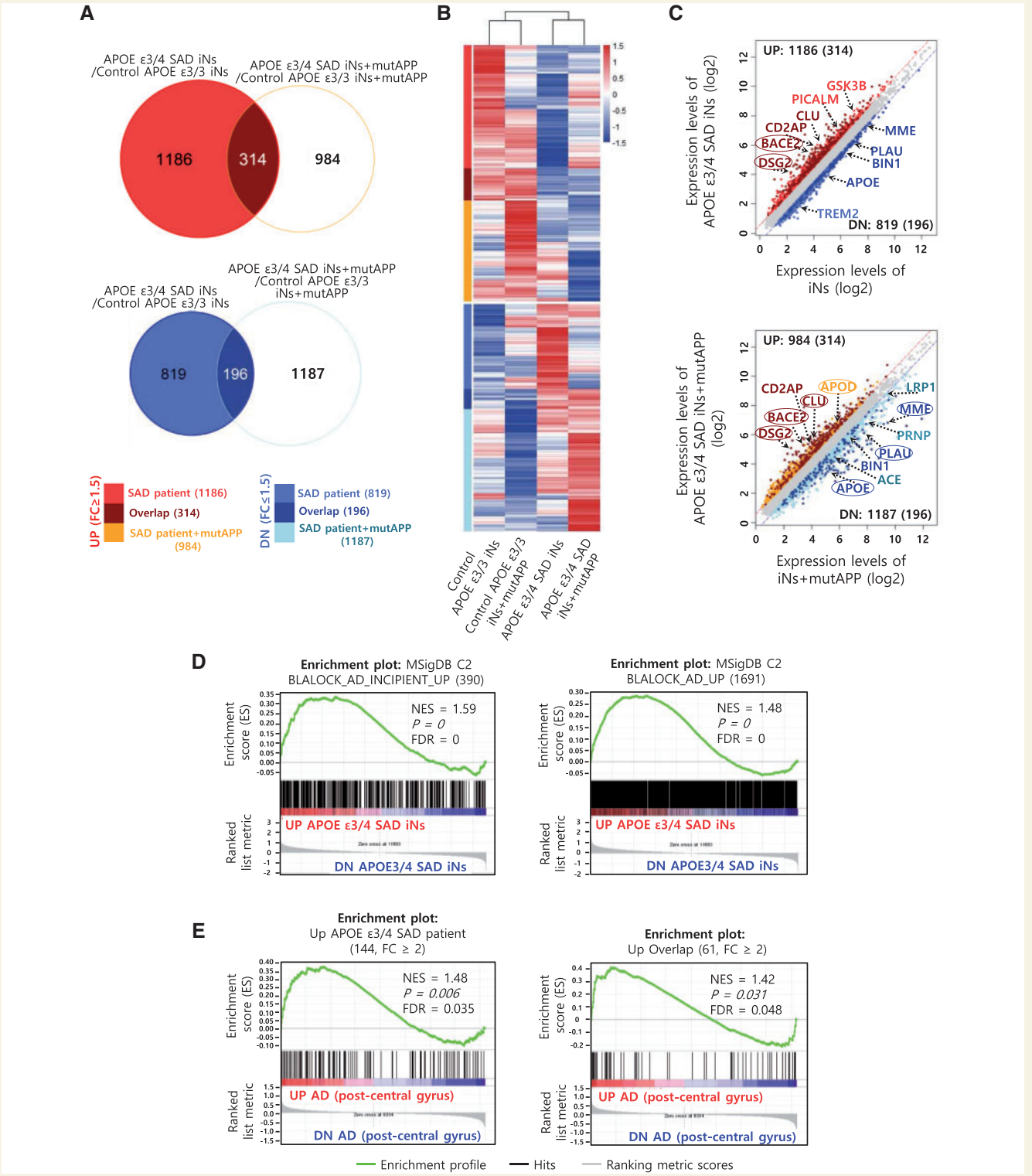

Figure 4 Global gene expression analysis of *APOE* ε3/4 patient (AG11414)-derived induced neurons and APOE ε3/3 control induced neurons. (**A**) Venn diagram showing the overlap of differentially expressed genes between sporadic Alzheimer's disease (*APOE* ε3/4) induced neurons (iNs) per *APOE* ε3/3 induced neurons and sporadic Alzheimer's disease (*APOE* ε3/4) induced neurons + mutAPP per *APOE* ε3/3 induced neurons + mutAPP. Number of 1.5 upregulated (*top*) and 1.5 downregulated (*middle*) gene are represented by specific group colour (*bottom*). (**B**) Heatmap showing microarray expression of differentially expressed genes. The column on the left represents specific group colour in **A**. (**C**) Scatter plot of the microarray expression data between *APOE* ε3/4 induced neurons and *APOE* ε3/3 induced neurons (*left*) and *APOE* ε3/4 induced neurons + mutAPP and APOE ε3/3 induced neurons + mutAPP (*right*). Up- and downregulated genes are presented as specific group colour based on **A**. Ellipses indicate 2-fold up- or 2-fold downregulated genes. (**D**) Gene set enrichment analysis of the microarray data from APOE ε3/4 induced neurons per APOE ε3/3 induced neurons. MSigDB C2 gene sets are used. (**E**) Gene set enrichment analysis of the microarray

(continued)

while other genes were not affected (Fig. 5F and Supplementary Fig. 5E).

To test whether DSG2 functionally contributes to *APOE* ε3/4-induced sporadic Alzheimer's disease phenotypes, we examined amyloid-β aggregation in APOE ε3/4 patient induced neurons upon DSG2 inhibition. Remarkably, we found that the increase in amyloid-β aggregation caused by APP overexpression in *APOE* ε3/4 patient induced neurons was effectively rescued by knockdown of DSG2 (Fig. 6A–C). Consistent with this result, the number of amyloid-β_{42}+ cells in the APP-expressing *APOE* ε3/4 induced neurons decreased upon *DSG2* knockdown, while expression of neuronal genes was not affected (Fig. 6D and Supplementary Fig. 6A). Moreover, these phenotypes were specific to the *APOE* ε3/4-associated Alzheimer's disease patient induced neurons and were absent from PSEN patient induced neurons (Supplementary Fig. 6B–D). We further demonstrated that accumulation of amyloid-β polymers in APP-expressing *APOE* ε3/4 patient induced neurons was significantly decreased by DSG2 inhibition (Fig. 5E and F). Consistent with this, overexpression of DSG2 in these *APP*-expressing *APOE* ε3/4 induced neurons increased amyloid-β aggregation (Supplementary Fig. 7A–E). Taken together, these data suggest that DSG2 mediates the *APOE* ε3/4-associated amyloid-β aggregation phenotypes in human induced neurons. Additionally, we found that the number of amyloid-β-positive puncta in APP-expressing *APOE* ε3/3 control induced neurons and *APOE* ε3/4 patient induced neurons are not affected by inhibition of β-secretase complexes (Supplementary Fig. 7A–E), suggesting that DSG2 is not their downstream target in APP processing.

Finally, we examined functional effects of DSG2 in the human *APOE* ε4- and APP-expressing mouse induced neurons. Consistent with the human data, elevated amyloid-β_{42} secretion in *Apoe* ε4- and *App*-expressing mouse induced neurons was significantly decreased by *Dsg2* knockdown (Fig. 6G–I). Moreover, we confirmed that transfection of *Dsg2* knockdown plasmids with GFP tags into mouse induced neurons led to a reduction in amyloid-β_{42} protein (Supplementary Fig. 8A and B), demonstrating a functional connection between APOE ε3/4 and DSG2, which may be critical for the control of APP processing in *APOE* ε3/4-associated sporadic Alzheimer's disease.

Discussion

Direct lineage reprogramming of fibroblasts into neurons by overexpressing key transcription factors is a conceptually intriguing strategy for modelling neurological diseases, since this technique has proved to be a rapid, robust and reproducible way to generate functional neurons (Vierbuchen *et al.*, 2010; Caiazzo *et al.*, 2011; Kim *et al.*, 2011; Wapinski *et al.*, 2013). Particularly, the generation of human induced neurons from patient fibroblasts represents a powerful tool for understanding pathological features of neurological diseases and screening for therapeutic interventions (Iovino *et al.*, 2014). However, the process of direct conversion of human fibroblasts into induced neurons by the transduction of transcription factors is highly inefficient, making it difficult to reproducibly and quantitatively characterize disease phenotypes in these cultures. Recently, a study reported the generation of chemically induced directly converted neurons from familial Alzheimer's disease patient fibroblasts that developed Alzheimer's disease pathological phenotypes (Hu *et al.*, 2015). To date, none of these studies have reported direct conversion of human induced neurons from sporadic patients with Alzheimer's disease. Thus, our study for the first time demonstrates the successful formation of sporadic Alzheimer's disease patient induced neurons with high efficiency using nanopatterned substrates. We further demonstrate the application of this culture platform in the discovery of novel pathogenic mechanisms that contribute to idiopathic sporadic Alzheimer's disease.

In the present study, we demonstrate that induced neurons derived from fibroblasts of mice, normal humans and patients with Alzheimer's disease can be used to model Alzheimer's disease. Murine induced neurons generated by the forced expression of *Ascl1*, *Brn2*, and *Myt1l* uniformly exhibit morphological and molecular features of glutamatergic forebrain neurons, and overexpression of mutant APP in these induced neurons recapitulates several pathological phenotypes associated with Alzheimer's disease, including abnormal accumulation of amyloid-β_{42} and altered tau protein phosphorylation. Notably, APP expressing human induced neurons recapitulated several abnormal Alzheimer's disease phenotypes, and these pathologies were reproduced in both mutant *APP*-expressing *APOE* ε3/4 patient induced neurons, suggesting that these Alzheimer's disease pathologies can be reproduced in directly converted human induced neurons. Consistent with this, these *APOE* ε3/4 patient induced neurons also exhibited vulnerability to peroxide-induced cell death. This is particularly interesting because the fibroblasts were derived from a patient with major Alzheimer's disease risk factor, *APOE* ε3/4 genotype, and the Alzheimer's disease pathological phenotype in *APOE* ε3/4 Alzheimer's disease patient-derived induced neurons demonstrate that

Figure 4 Continued

data from Alzheimer's disease patient (*APOE* ε3/4 genotype) datasets in human post-central gyrus (GSE48350). Sets of the upregulated (fold change ⩾ 2) genes based on *APOE* ε3/4 induced neurons per *APOE* ε3/3 induced neurons are used. The *APOE* ε3/4 patient post-central gyrus datasets were enriched in upregulated overlap genes between *APOE* ε3/4 induced neurons and APP-expressing *APOE* ε3/4 induced neurons. SAD = sporadic Alzheimer's disease.

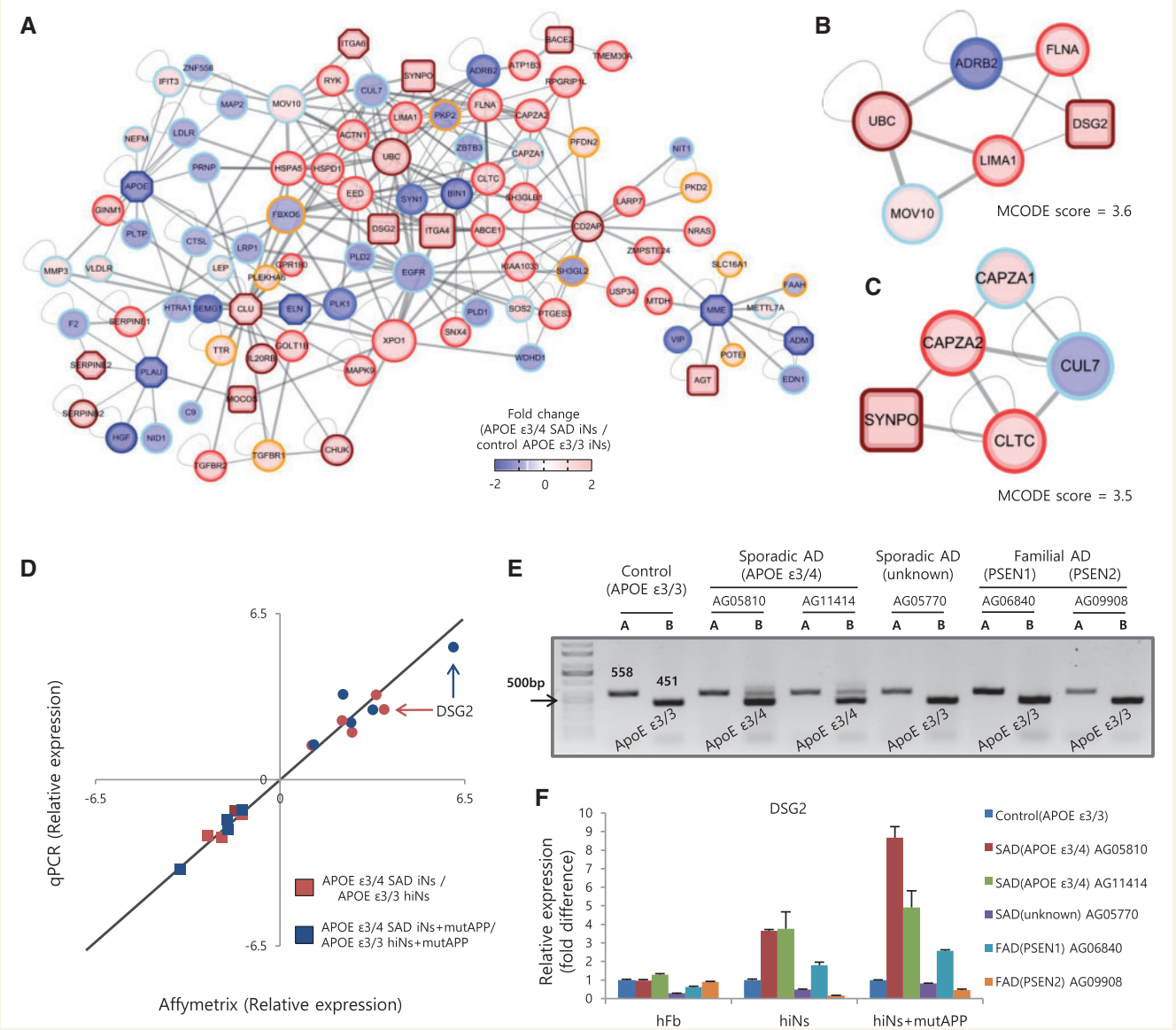

Figure 5 Protein–protein interaction networks in sporadic Alzheimer's disease *APOE* ε3/4 patient-derived induced neurons. (**A**) Protein–protein interaction network. A subnetwork showing direct interaction with proteins encoded by upregulated overlap genes (*DSG2*, *BACE2*, *CLU*, *CD2AP*) and downregulated overlap genes (*APOE*, *BIN1*, *PLAU*, *MME*) in Fig. 4A and C. Node or edge size indicate degrees or edge-between, respectively. The ellipse-shaped nodes indicate proteins and rectangle shaped nodes represent proteins that have fold-change ⩾ 2 in *APOE* ε3/4 induced neurons per APOE ε3/3 induced neurons and *APOE* ε3/4 induced neurons + mutAPP per *APOE* ε3/3 induced neurons + mutAPP. Node border colour represents specific group colour as shown in Fig. 4A. (**B** and **C**) Molecular Complex Detection analysis results from **A** showing 3.6 (**B**) and 3.5 (**C**) molecular complex detection score. (**D**) Validation of gene expression between microarray data and qRT-PCR. (**E**) Validation of *APOE* genotypes in human fibroblasts and Alzheimer's disease patient fibroblasts. Mixture A includes genotype primers against Cys112 (558 bp) and Cys158 (451 bp). Mixture B includes genotype primers against Arg112 (588 bp) and Arg158 (451 bp). (**F**) qRT-PCR analysis of DSG2 expression in human fibroblasts, human induced neurons and APP expressing human induced neurons about control fibrobalst, AG05810, AG11414, AG05770, AG06840 and AG09908. hFb = human fibroblasts; FAD = familial Alzheier's disease; iNs = induced neurons; SAD = sporadic Alzheimer's disease.

characteristics of Alzheimer's disease are retained in the directly reprogrammed neurons. More importantly, a significant number of genes that were differentially expressed in *APOE* ε3/4 Alzheimer's disease patient induced neurons was also enriched in the sporadic Alzheimer's disease patient brain database, suggesting that this strategy can be used for identifying new disease interventions and for drug screening for Alzheimer's disease.

Remarkably, we identify a direct functional connection between *APOE* ε3/4 and another Alzheimer's disease susceptibility locus, which might contribute to the disease phenotypes in *APOE* ε3/4 sporadic patients with

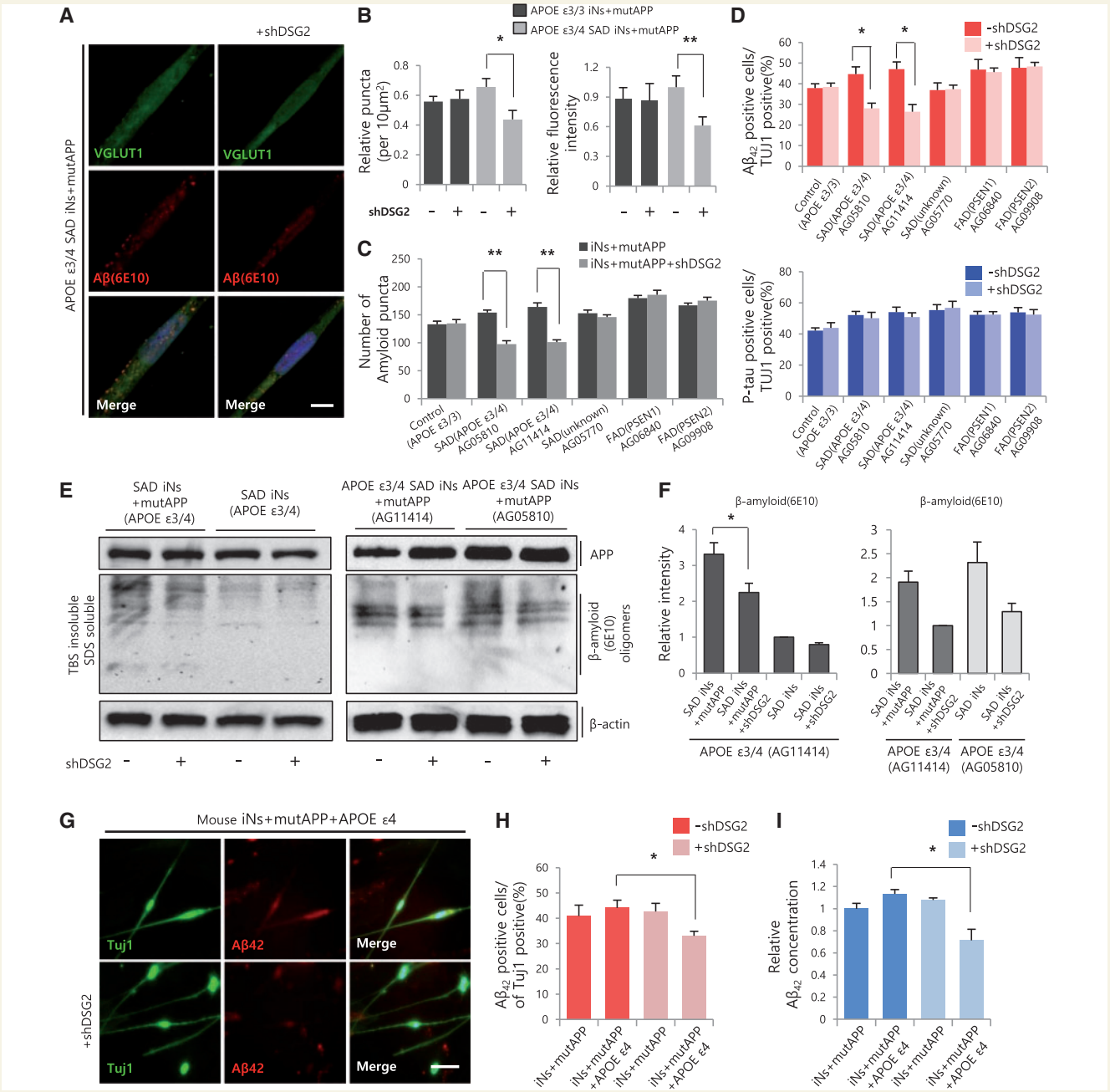

Figure 6 Knockdown of *DSG2* decreases amyloid-β peptides in *APOE* ε3/4 patient cell lines and APP expressing *APOE* ε4 mouse induced neurons. (**A**) Immunofluorescence of VGLUT1 and amyloid-β (6E10) in sporadic Alzheimer's disease patient (*APOE* ε3/4 genotype) APP expressing induced neurons (iNs) and DSG2 knockdown. Scale bar = 10 μm. (**B**) Analysis of relative amyloid puncta (*left*) and fluorescence intensity (*right*) in APP expressing *APOE* ε3/4 patient induced neurons and APP expressing *APOE* ε3/4 patient induced neurons treated with *DSG2*-shRNA. Data represent mean ± SEM. Student's *t*-test, $^{*}P < 0.05$, $^{**}P < 0.01$; $n = 6$ per sample. (**C**) Number of amyloid puncta per cell was decreased in *APOE* ε3/4 patient cells (AG05810 and AG11414), but *APOE* ε3/3 patient cells do not. Data represent mean ± SEM. Student's *t*-test, $^{*}P < 0.05$, $^{**}P < 0.01$; $n = 6$ per each sample. (**D**) Analysis of amyloid-β_{42}/TUJ1 (*top*) and P-TAU/TUJ1 (*bottom*) -positive cells in patient induced neurons and APP expressing patient induced neurons treated with *DSG2*-shRNA about control human cell line and five patient cell lines. Data represent mean ± SEM. Student's *t*-test, $^{*}P < 0.05$, $^{**}P < 0.01$; $n = 6$ per each sample. (**E** and **F**) Western blot analysis for APP and amyloid-β (6E10) shows reduction of amyloid-β oligomers in APP expressing sporadic Alzheimer's disease patient (*APOE* ε3/4 genotype) induced neurons treated with *DSG2*-shRNA. Data represent mean ± SEM. Student's *t*-test, $^{*}P < 0.05$. (**G**) Immunostaining analysis of the intracellular accumulation of amyloid-β_{42} in APP and human APOE (hAPOE) ε4 expressing mouse induced neurons. Scale bar = 100 μm. (**H**) The percentage of amyloid-β_{42}/TUJ1 positive APP expressing *Apoe* ε4 mouse induced neurons on 10 days after doxycycline induction. Data represent mean ± SEM. Student's *t*-test, $^{*}P < 0.05$, $^{**}P < 0.01$ $n = 6$ per each sample. (**I**) ELISA analysis of the intracellular amyloid-β_{42} secreted from APP expressing mouse induced neurons and APP expressing APOE ε4 mouse induced neurons treated with shDSG2. Data represent mean ± SEM. ANOVA test, $^{*}P < 0.05$, $^{**}P < 0.01$; $n = 6$ per each sample. SAD = sporadic Alzheimer's disease.

Alzheimer's disease. Analysis of the subnetworks within differentially expressed genes from *APOE* ε3/4 patient-derived induced neurons revealed, that the DSG2 complex is closely related to the *APOE* ε3/4-induced Alzheimer's disease phenotypes. While it has been recently reported that the polymorphisms in *DSG2* are associated with sporadic Alzheimer's disease through gene-wide association study, the functional connection between DSG2 and APOE ε3/4 was not previously known. We further demonstrated that this functional connection between APOE ε3/4 and DSG2 was specific for *APOE* ε3/4-associated sporadic Alzheimer's disease by examining Alzheimer's disease pathological phenotypes in healthy normal and other Alzheimer's disease patient-derived induced neuron lines. This is the first report of a functional connection between genetic loci linked to sporadic Alzheimer's disease. The identification of functional connections between Alzheimer's disease disease-linked genes provides important insight into the pathophysiology of Alzheimer's disease development and highlights cellular pathways upon which these gene products may converge. These pathways may represent promising therapeutic targets for the treatment of Alzheimer's disease. Thus, our study elucidating the mechanisms affected by genetic variants identified by gene-wide association study using induced neurons represents a novel approach for the development of personalized medicine for more effective treatments of sporadic Alzheimer's disease.

Funding

This work was supported by the National Research Foundation funded by the Korea government (NRF-2017M3A9C6029306, 2016R1A2B2014195, 2015R1A2A1A01003530, 2015M3A9C7030128), Korea Health Technology R&D Project, Ministry of Health & Welfare (HI16C1176), the Next-Generation BioGreen 21 Program, Rural Development Administration (PJ0110770) and the Ministry of Food and Drug Safety in 2017 (14172MFDS974).

Supplementary material

Supplementary material is available at *Brain* online.

References

Ambasudhan R, Talantova M, Coleman R, Yuan X, Zhu S, Lipton SA, et al. Direct reprogramming of adult human fibroblasts to functional neurons under defined conditions. Cell Stem Cell 2011; 9: 113–8.

Arber C, Precious SV, Cambray S, Risner-Janiczek JR, Kelly C, Noakes Z, et al. Activin A directs striatal projection neuron differentiation of human pluripotent stem cells. Development 2015; 142: 1375–86.

Bader GD, Hogue CW. An automated method for finding molecular complexes in large protein interaction networks. BMC Bioinformatics 2003; 4: 2.

Caiazzo M, Dell'Anno MT, Dvoretskova E, Lazarevic D, Taverna S, Leo D, et al. Direct generation of functional dopaminergic neurons from mouse and human fibroblasts. Nature 2011; 476: 224–7.

Choi SH, Kim YH, Hebisch M, Sliwinski C, Lee S, D'Avanzo C, et al. A three-dimensional human neural cell culture model of Alzheimer's disease. Nature 2014; 515: 274–8.

Citron M, Eckman CB, Diehl TS, Corcoran C, Ostaszewski BL, Xia W, et al. Additive effects of PS1 and APP mutations on secretion of the 42-residue amyloid β-protein. Neurobiol Dis 1998; 5: 107–16.

Cremades N, Cohen Samuel IA, Deas E, Abramov Andrey Y, Chen Allen Y, Orte A, et al. Direct observation of the interconversion of normal and toxic forms of α-synuclein. Cell 2012; 149: 1048–59.

Duan L, Bhattacharyya BJ, Belmadani A, Pan L, Miller RJ, Kessler JA. Stem cell derived basal forebrain cholinergic neurons from Alzheimer's disease patients are more susceptible to cell death. Mol Neurodegener 2014; 9: 3.

Efe JA, Hilcove S, Kim J, Zhou H, Ouyang K, Wang G, et al. Conversion of mouse fibroblasts into cardiomyocytes using a direct reprogramming strategy. Nat Cell Biol 2011; 13: 215–22.

Frackowiak J, Miller DL, Potempska A, Sukontasup T, Mazur-Kolecka B. Secretion and accumulation of Abeta by brain vascular smooth muscle cells from AbetaPP-Swedish transgenic mice. J Neuropathol Exp Neurol 2003; 62: 685–96.

Glenner GG, Wong CW, Quaranta V, Eanes ED. The amyloid deposits in Alzheimer's disease: their nature and pathogenesis. Appl Pathol 1984; 2: 357–69.

Gotz J, Probst A, Spillantini MG, Schafer T, Jakes R, Burki K, et al. Somatodendritic localization and hyperphosphorylation of tau protein in transgenic mice expressing the longest human brain tau isoform. EMBO J 1995; 14: 1304–13.

HD iPSC Consortium. Induced pluripotent stem cells from patients with Huntington's disease show CAG-repeat-expansion-associated phenotypes. Cell Stem Cell 2012; 11: 264–78.

Hu W, Qiu B, Guan W, Wang Q, Wang M, Li W, et al. Direct conversion of normal and Alzheimer's disease human fibroblasts into neuronal cells by small molecules. Cell Stem Cell 2015; 17: 204–12.

Ieda M, Fu JD, Delgado-Olguin P, Vedantham V, Hayashi Y, Bruneau BG, et al. Direct reprogramming of fibroblasts into functional cardiomyocytes by defined factors. Cell 2010; 142: 375–86.

Iovino M, Pfisterer U, Holton JL, Lashley T, Swingler RJ, Calo L, et al. The novel MAPT mutation K298E: mechanisms of mutant tau toxicity, brain pathology and tau expression in induced fibroblast-derived neurons. Acta Neuropathol 2014; 127: 283–95.

Israel MA, Yuan SH, Bardy C, Reyna SM, Mu Y, Herrera C, et al. Probing sporadic and familial Alzheimer's disease using induced pluripotent stem cells. Nature 2012; 482: 216–20.

Karch CM, Goate AM. Alzheimer's disease risk genes and mechanisms of disease pathogenesis. Biol Psychiatry 2015; 77: 43–51.

Kim J, Basak JM, Holtzman DM. The role of apolipoprotein E in Alzheimer's disease. Neuron 2009; 63: 287–303.

Kim J, Su SC, Wang H, Cheng AW, Cassady JP, Lodato MA, et al. Functional integration of dopaminergic neurons directly converted from mouse fibroblasts. Cell Stem Cell 2011; 9: 413–9.

Koffie RM, Hashimoto T, Tai HC, Kay KR, Serrano-Pozo A, Joyner D, et al. Apolipoprotein E4 effects in Alzheimer's disease are mediated by synaptotoxic oligomeric amyloid-beta. Brain 2012; 135(Pt 7): 2155–68.

Kondo T, Asai M, Tsukita K, Kutoku Y, Ohsawa Y, Sunada Y, et al. Modeling Alzheimer's disease with iPSCs reveals stress phenotypes associated with intracellular Abeta and differential drug responsiveness. Cell Stem Cell 2013; 12: 487–96.

Lambert JC, Ibrahim-Verbaas CA, Harold D, Naj AC, Sims R, Bellenguez C, et al. Meta-analysis of 74,046 individuals identifies 11 new susceptibility loci for Alzheimer's disease. Nat Genet 2013; 45: 1452–8.

Lee MR, Kwon KW, Jung H, Kim HN, Suh KY, Kim K, et al. Direct differentiation of human embryonic stem cells into selective neurons on nanoscale ridge/groove pattern arrays. Biomaterials 2010; 31: 4360–6.

Marro S, Pang ZP, Yang N, Tsai MC, Qu K, Chang HY, et al. Direct lineage conversion of terminally differentiated hepatocytes to functional neurons. Cell Stem Cell 2011; 9: 374–82.

Mayeux R, Saunders AM, Shea S, Mirra S, Evans D, Roses AD, et al. Utility of the apolipoprotein E genotype in the diagnosis of Alzheimer's disease. Alzheimer's Disease Centers Consortium on Apolipoprotein E and Alzheimer's Disease. N Engl J Med 1998; 338: 506–11.

Meyer K, Ferraiuolo L, Miranda CJ, Likhite S, McElroy S, Renusch S, et al. Direct conversion of patient fibroblasts demonstrates non-cell autonomous toxicity of astrocytes to motor neurons in familial and sporadic ALS. Proc Natl Acad Sci USA 2014; 111: 829–32.

Muratore CR, Rice HC, Srikanth P, Callahan DG, Shin T, Benjamin LN, et al. The familial Alzheimer's disease APPV717I mutation alters APP processing and Tau expression in iPSC-derived neurons. Hum Mol Genet 2014; 23: 3523–36.

Pan F, Zhang M, Wu G, Lai Y, Greber B, Scholer HR, et al. Topographic effect on human induced pluripotent stem cells differentiation towards neuronal lineage. Biomaterials 2013; 34: 8131–9.

Pfisterer U, Kirkeby A, Torper O, Wood J, Nelander J, Dufour A, et al. Direct conversion of human fibroblasts to dopaminergic neurons. Proc Natl Acad Sci USA 2011; 108: 10343–8.

Raja WK, Mungenast AE, Lin YT, Ko T, Abdurrob F, Seo J, et al. Self-organizing 3D human neural tissue derived from induced pluripotent stem cells recapitulate Alzheimer's disease phenotypes. PLoS One 2016; 11: e0161969.

Ravichandran R, Liao S, Ng C, Chan CK, Raghunath M, Ramakrishna S. Effects of nanotopography on stem cell phenotypes. World J Stem Cells 2009; 1: 55–66.

Reiman EM, Caselli RJ, Yun LS, Chen K, Bandy D, Minoshima S, et al. Preclinical evidence of Alzheimer's disease in persons homozygous for the epsilon 4 allele for apolipoprotein E. N Engl J Med 1996; 334: 752–8.

Selkoe DJ. Alzheimer's disease is a synaptic failure. Science 2002; 298: 789–91.

Selkoe DJ. DEfining molecular targets to prevent Alzheimer disease. Arch Neurol 2005; 62: 192–5.

Serneels L, Van Biervliet J, Craessaerts K, Dejaegere T, Horre K, Van Houtvin T, et al. gamma-Secretase heterogeneity in the Aph1 subunit: relevance for Alzheimer's disease. Science 2009; 324: 639–42.

Shannon P, Markiel A, Ozier O, Baliga NS, Wang JT, Ramage D, et al. Cytoscape: a software environment for integrated models of biomolecular interaction networks. Genome Res 2003; 13: 2498–504.

Shen J, Kelleher RJ 3rd. The presenilin hypothesis of Alzheimer's disease: evidence for a loss-of-function pathogenic mechanism. Proc Natl Acad Sci USA 2007; 104: 403–9.

Shi Y, Kirwan P, Smith J, MacLean G, Orkin SH, Livesey FJ. A human stem cell model of early Alzheimer's disease pathology in Down syndrome. Sci Transl Med 2012; 4: 124ra29.

Singleton AB, Hall R, Ballard CG, Perry RH, Xuereb JH, Rubinsztein DC, et al. Pathology of early-onset Alzheimer's disease cases bearing the Thr113-114ins presenilin-1 mutation. Brain 2000; 123 (Pt 12): 2467–74.

Solanki A, Shah S, Yin PT, Lee KB. Nanotopography-mediated reverse uptake for siRNA delivery into neural stem cells to enhance neuronal differentiation. Sci Rep 2013; 3: 1553.

Subramanian A, Tamayo P, Mootha VK, Mukherjee S, Ebert BL, Gillette MA, et al. Gene set enrichment analysis: a knowledge-based approach for interpreting genome-wide expression profiles. Proc Natl Acad Sci USA 2005; 102: 15545–50.

Tanzi RE, Moir RD, Wagner SL. Clearance of Alzheimer's Aβ peptide: the many roads to perdition. Neuron 2004; 43: 605–8.

Teasdale GM, Murray GD, Nicoll JA. The association between APOE epsilon4, age and outcome after head injury: a prospective cohort study. Brain 2005; 128 (Pt 11): 2556–61.

Thinakaran G, Koo EH. Amyloid precursor protein trafficking, processing, and function. J Biol Chem 2008; 283: 29615–9.

Vetrivel KS, Zhang X, Meckler X, Cheng H, Lee S, Gong P, et al. Evidence that CD147 modulation of β-amyloid (Aβ) levels is mediated by extracellular degradation of secreted Aβ. J Biol Chem 2008; 283: 19489–98.

Vierbuchen T, Ostermeier A, Pang ZP, Kokubu Y, Sudhof TC, Wernig M. Direct conversion of fibroblasts to functional neurons by defined factors. Nature 2010; 463: 1035–41.

Vierbuchen T, Wernig M. Direct lineage conversions: unnatural but useful[quest]. Nat Biotech 2011; 29: 892–907.

Wapinski OL, Vierbuchen T, Qu K, Lee QY, Chanda S, Fuentes DR, et al. Hierarchical mechanisms for direct reprogramming of fibroblasts to neurons. Cell 2013; 155: 621–35.

Wolfe MS, Xia W, Ostaszewski BL, Diehl TS, Kimberly WT, Selkoe DJ. Two transmembrane aspartates in presenilin-1 required for presenilin endoproteolysis and [gamma]-secretase activity. Nature 1999; 398: 513–7.

Yang N, Zuchero JB, Ahlenius H, Marro S, Ng YH, Vierbuchen T, et al. Generation of oligodendroglial cells by direct lineage conversion. Nat Biotechnol 2013; 31: 434–9.

Yoo J, Noh M, Kim H, Jeon NL, Kim BS, Kim J. Nanogrooved substrate promotes direct lineage reprogramming of fibroblasts to functional induced dopaminergic neurons. Biomaterials 2015; 45: 36–45.

Young JE, Boulanger-Weill J, Williams DA, Woodruff G, Buen F, Revilla AC, et al. Elucidating molecular phenotypes caused by the SORL1 Alzheimer's disease genetic risk factor using human induced pluripotent stem cells. Cell Stem Cell 2015; 16: 373–85.